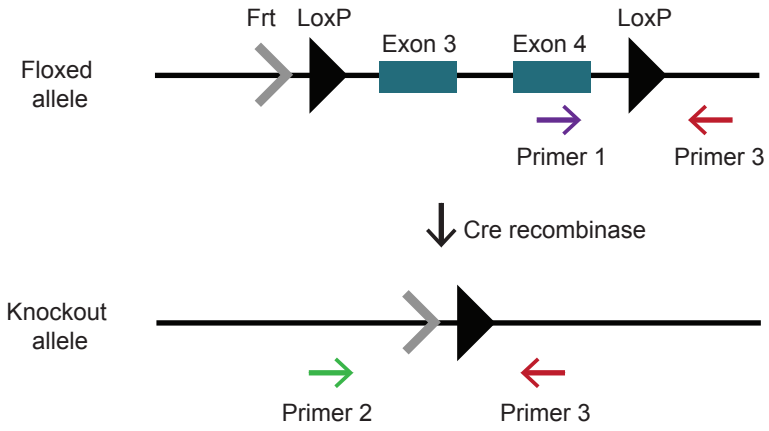

350 bp amplicon from primers 1+3 detects undeleted floxed allele
448 bp amplicon from primers 2+3 detects deletion of floxed allele

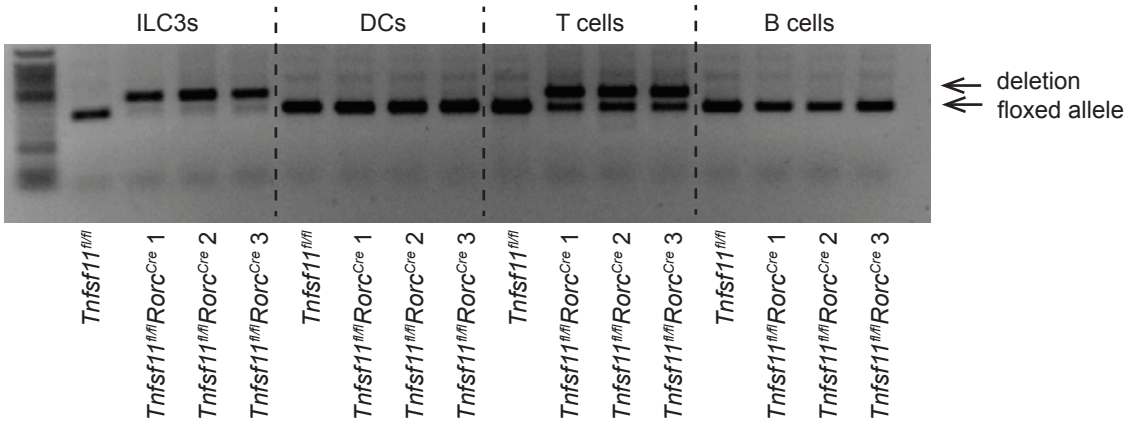

Figure S1. Assessment of *Tnfsf11* deletion in *Tnfsf11*$^{fl/fl}$*Rorc*^{Cre} small intestine lamina propria ILC3s, dendritic cells (DC), T cells, and B cells by genomic PCR. Related to Figure 1.

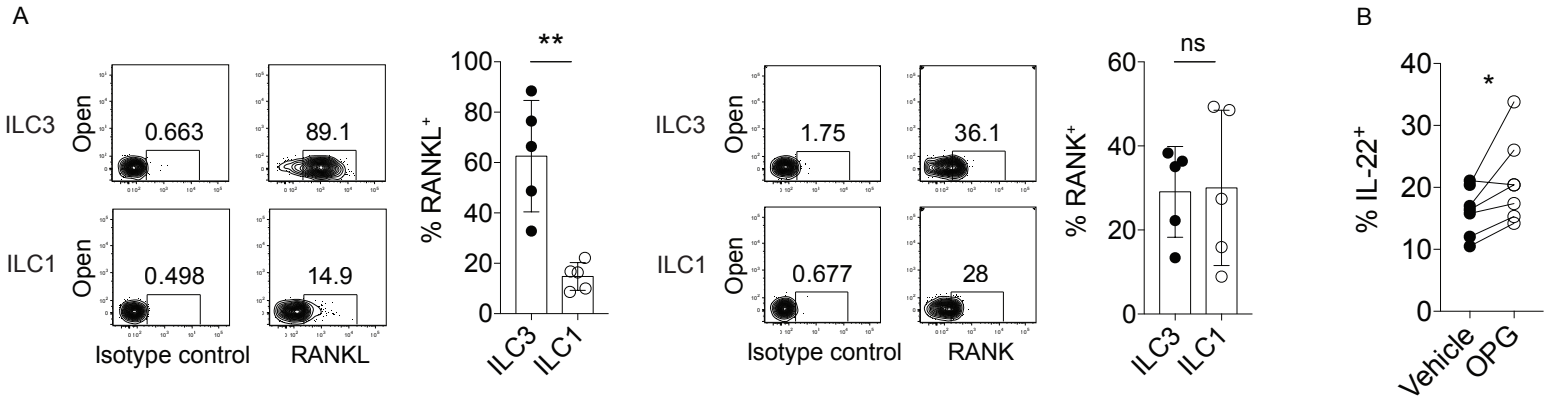

Figure S2. RANK and RANKL in human tonsil. Related to Figure 4. (A) anti-RANKL and anti-RANK staining in ILC3 and ILC1 isolated from human tonsils (n=5 donors). (B) IL-22 production in sorted tonsil ILC3s pre-treated with OPG prior to stimulation with IL-23 and IL-1β (n=7 donors). Bars indicate mean (+/- s.d). *P ≤0.05, **P≤0.01.

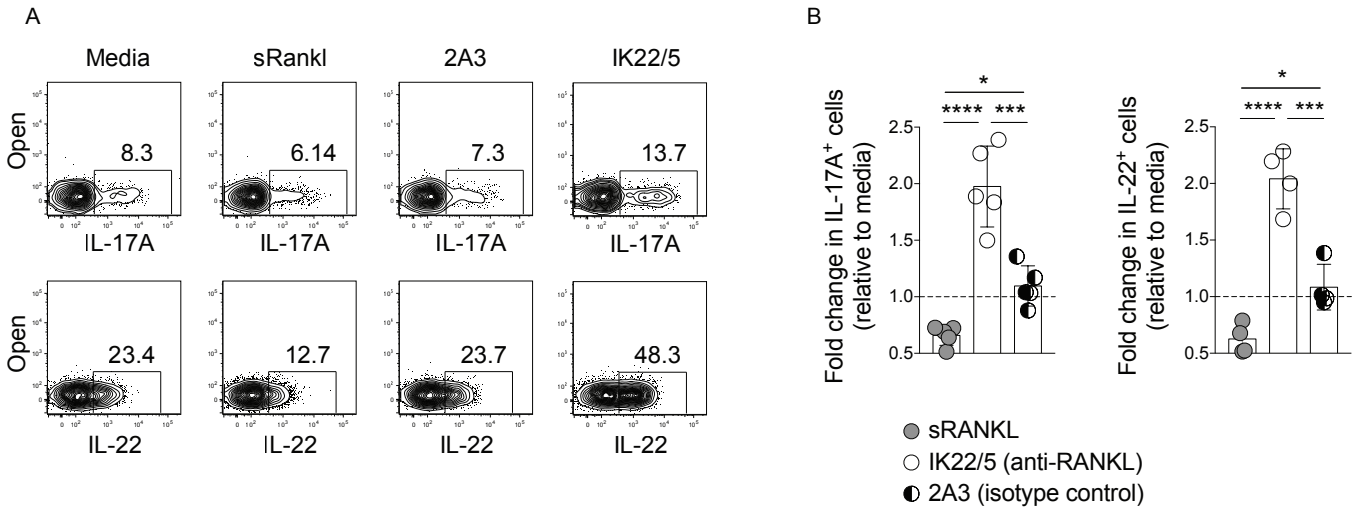

Figure S3. Effects of RANK-RANKL interactions in MNK-3 cells. Related to Figure 4. (A) Representative FACS plots and (B) quantification of IL-23 and IL-1β-elicited IL-17A and IL-22 by MNK-3 cells pre-treated with soluble RANKL, isotype control antibody, or anti-RANKL antibody. Each dot represents an independent experiment. Bars indicate mean (+/- s.d). *P≤0.05, ***P≤0.001, ****P≤0.0001.

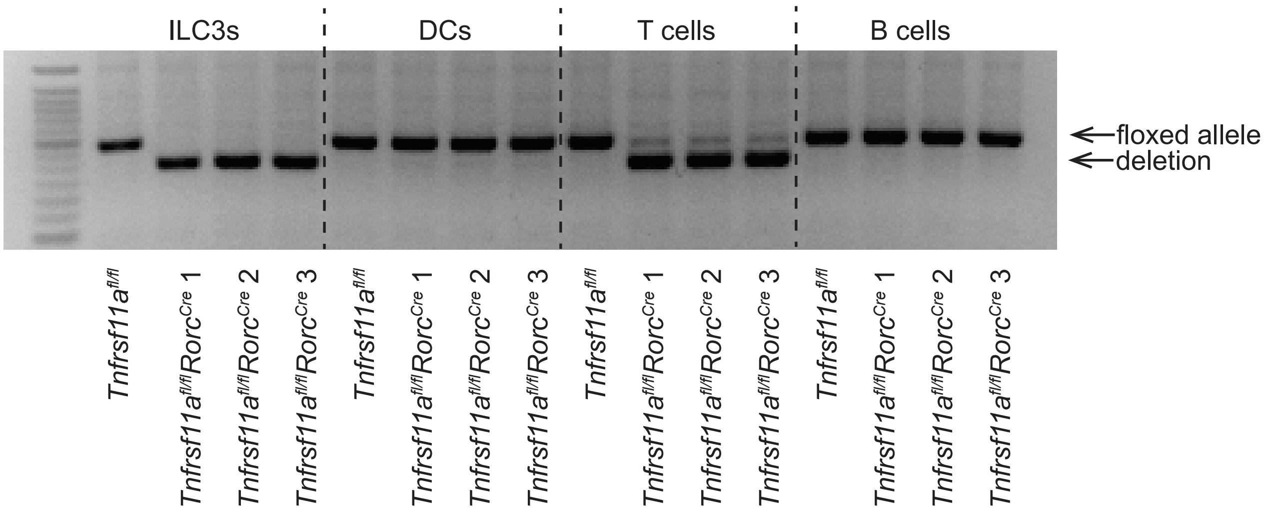

Figure S4. Assessment of *Tnfrsf11a* deletion in *Tnfrsf11a*$^{fl/fl}$ *Rorc*^{Cre} small intestine lamina propria ILC3s, DCs, T cells, and B cells by genomic PCR. Related to Figure 5.

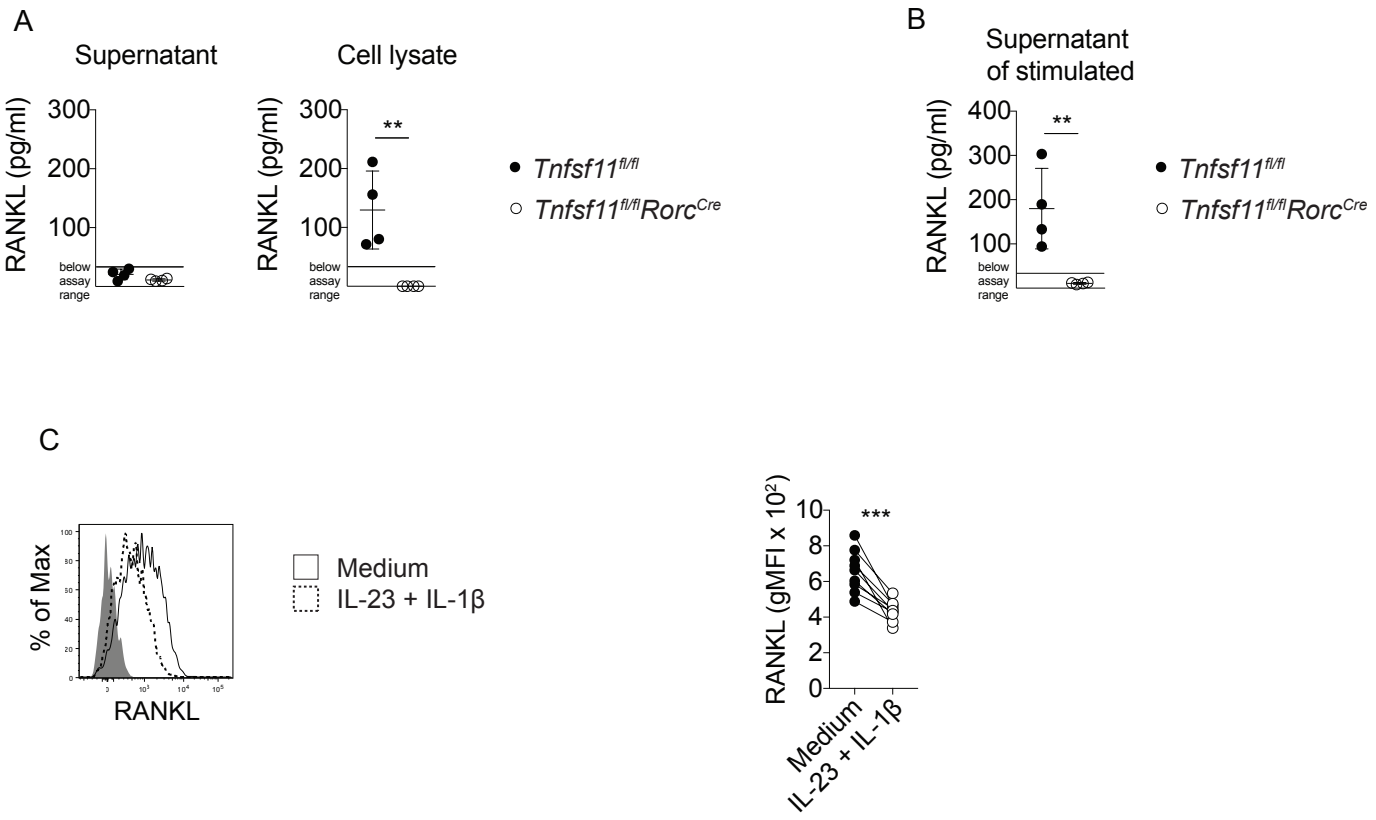

Figure S5. RANKL shedding by ILC3. Related to Figure 5. (A) RANKL detected by ELISA in supernatants or cell lysates of sorted small intestine CCR6^{+} ILC3s after 3 d in culture with IL-7. (B) RANKL detected by ELISA in supernatants of sorted small intestine CCR6^{+} ILC3s after 3 d in culture with IL-7, IL-23, and IL-1β. (C) Representative plot (left) and quantified geometric MFI (right) of cell surface RANKL staining in sorted small intestine CCR6^{+} ILC3s 5 h after culture with IL-23 and IL-1β. The shaded histogram represents RANKL-antibody stained *Tnfsf11*$^{-/-}$ cells. Bars indicate mean (+/- s.d). **P≤0.01, ***P≤0.001.

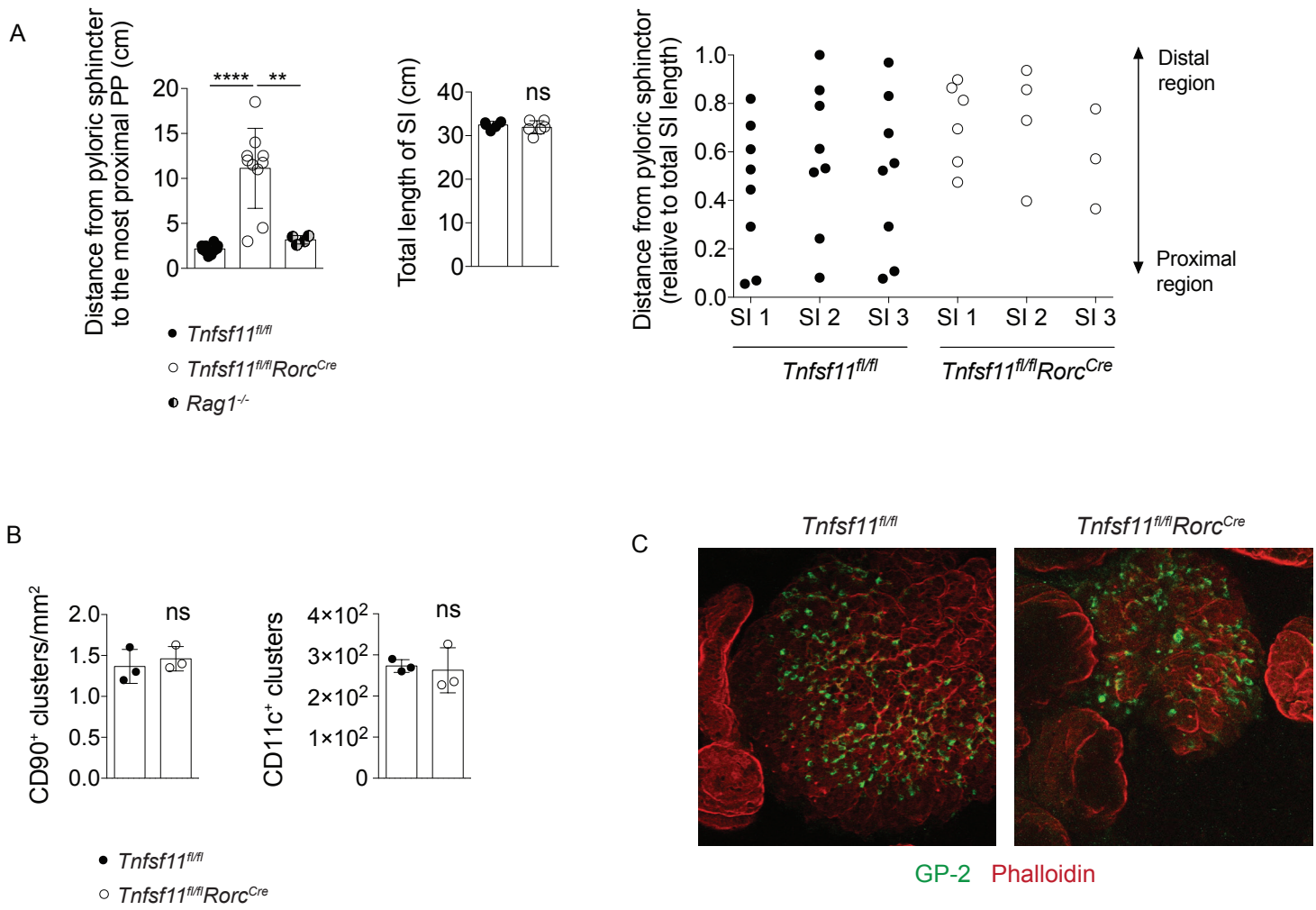

Figure S6. Lymphoid structures and M cell development in *Tnfsf11*$^{fl/fl}$*Rorc*^{Cre} mice. Related to Figure 6. (A) (Left) Distance from the pyloric sphincter to the most proximal Peyer's patch along the small intestine in *Tnfsf11*$^{fl/fl}$, *Tnfsf11*$^{fl/fl}$*Rorc*^{Cre}, and *Rag1*$^{-/-}$ mice. (Middle) Total length of small intestines (SI) from *Tnfsf11*$^{fl/fl}$ and *Tnfsf11*$^{fl/fl}$*Rorc*^{Cre} mice. (Right) Distance from the pyloric sphincter to each Peyer's patch in 3 *Tnfsf11*$^{fl/fl}$ and 3 *Tnfsf11*$^{fl/fl}$*Rorc*^{Cre} mice, relative to the length of the small intestine. Each dot represents a single Peyer's patch. (B) Quantification of gut tertiary lymphoid organs in *Tnfsf11*$^{fl/fl}$ and *Tnfsf11*$^{fl/fl}$*Rorc*^{Cre} mice. Cryptopatches were identified as CD90^{+} cell clusters. CD11c^{+} cell clusters were used to identify a spectrum of lymphoid structures that included CD11c^{+} cell-containing intermediate cryptopatch stages and isolated lymphoid follicles. (C) Whole mount GP-2 staining on FAE of ileal Peyer's patches in *Tnfsf11*$^{fl/fl}$ or *Tnfsf11*$^{fl/fl}$*Rorc*^{Cre} mice. Bars indicate mean (+/- s.d). **P≤0.01, ****P≤0.0001.